Research Report

KSTS/RR-05/005
Oct. 12, 2005

New Method of ground reflection coefficient reconstruction and Shape recovery by SAR signal modeling

by

Yoshimitsu Aoki and Takeshi Kato

Yoshimitsu Aoki
Graduate School of International Corporate Strategy
Hitotsubashi University
and
Takeshi Kato
Department of Mathematics
Keio University

Department of Mathematics
Faculty of Science and Technology
Keio University

3-14-1 Hiyoshi, Kohoku-ku, Yokohama, 223-8522 Japan

KSTS/RR-05/005
October 12, 2005

New method of ground reflection coefficient reconstruction and shape recovery by another SAR signal modeling

Yoshimitsu Aoki
Graduate School of International Corporate Strategy,
Hitotsubashi University
2-1-2 Hitotsubashi Chiyoda Tokyo, Japan
Zip code: 101-8439
Phone: +81-3-4212-3018
e-mail address: yaoki@ics.hit-u.ac.jp

Takeshi Kato
Department of Mathematics,
Keio University
3-14-1 Hiyoshi Kohoku Yokohama, Japan
Zip code: 223-8522
Phone: +81-45-566-1423
e-mail address: tkato@math.keio.ac.jp

Abstract

This paper proposes a new method to reconstruct the reflection coefficient of the ground surface from synthetic aperture radar signal. The received signal is modeled in more general and natural form than the point targets model. By introducing a polar coordinate system and analyzing the model rigorously, two kinds of operators are derived. The reconstruction method consists of applying these operators to received signal in order. The new method is superior to the conventional pulse compression technique in three points: the simplicity of the calculation for reconstruction itself, built-in correction function without post process, and shape recovery with high resolution. The theoretical background of the method is proved rigorously and numerical examples are presented to show the advantages of the method. The sensitivity to noise is also investigated through obtaining the upper bound of the noise level theoretically and a numerical work.

Keyword : SAR signal; Ground reflection coefficient; Shape recovery; Pulse compression; Additive noise

1 Introduction

Synthetic aperture radar (SAR) has been used in various fields such as geology, oceanography, botany, agriculture, meteorology, disaster prediction, and so forth, and now we can make use of information about them easily. Since SAR system was developed by C. Wiley in 1952 ([14]), so many new technologies and countless research papers have been presented. Inverse SAR, Interferometric SAR and Polarimetric SAR are examples of the former ([3], [9]), and the theory of the pulse compression technique for higher resolution is one of the most important results of the latter ([2], [3], [6], [9]). Research works are still going on accompanied by the rapid progress of computer technologies and electronic devices. For example, a method of detecting a ground moving target by using an eigendecomposition of the multi-channel covariance matrix is presented in [12], new techniques to improve the geometric resolution for polarimetric SAR images are proposed in [11] as an application of parametric spectral estimates, and so on.

As seen in [7], [8], [13] and some papers above, various methods have been developed in the framework of the pulse compression technique. The fundamental assumption in the technique is the point targets model. This model expresses received signal as a sum of returned signals from each target point, so that the manipulation of received signal for higher resolution, such as matched filtering and compression by using Doppler frequency, becomes easy. In the recent usage of satellite SAR system, however, targets on the ground are usually objects having shapes and areas rather than points. In this case, the point targets model is not necessarily appropriate because it discretizes the reflection coefficient of the ground surface by points and therefore fails to preserve the information about shapes and areas. That kind of information is recovered in post process such as distortion correction, location correction, and modification by prior information. From a different point of view, this fact suggests that shapes and areas can be recovered to some extent without post process if the reflection coefficient is modeled so as to preserve the information of those and the reconstruction method is derived based on such a model.

Then we begin our argument with modeling of the reflection coefficient in more appropriate form than point targets model. Our modeling preserves the information dropped in the point target model, since we do not discretize the reflection coefficient. Analyzing the model rigorously on the polar coordinate system, we derive two kinds of difference-based operators. The reconstruction method consisting of these operators has advantages over the conventional pulse compression technique in the following points: the simplicity of the calculation for reconstruction itself, built-in correction function without post process, and shape recovery with high resolution. The method is quite simple. Essentially we have only to make difference calculations of received signal.

The rest of this paper is organized as follows. In Section 2, formulation of the problem including the modeling of SAR signal is described. In Section 3, we state main theoretical results in the form of two theorems and propose a method to reconstruct the reflection coefficient based on these theorems. Section 4 gives numerical examples by using the parameters of a SAR system satellite operated practically. In this section, the comparison with the conventional range and azimuth compression technique is made and the sensitivity to noise is also investigated. Then we close the argument by concluding remarks in Section 5. The proofs of the theorems and a preliminary result are given in Appendices separately.

2 Formulation of the problem

2.1 Basic Geometry

Let us introduce an orthogonal three dimensional coordinate system (x, y, z). We suppose that the location of the satellite is denoted by $(x, 0, h_0)$, where $h_0 > 0$ is the height of the satellite and we assume that $x \geq 0$ by letting the starting point of the satellite be $x = 0$.

(Figure 1: Relationship between the satellite and a point on the ground)

For simplicity, let the ground surface be xy-plain. Then the reflection coefficient of the ground is described as a function of two variables (x, y), therefore we denote the reflection coefficient at the point (x, y) by $A(x, y)$. We may assume $y > 0$ also from the property of sideway looking radar system.

2.2 Modeling of the Radar Signal

Let the signal transmitted at time t be

$$s(t) := \exp\{i(\omega_0 t + \beta t^2)\} I_{(0,T]}(t), \tag{1}$$

where $\omega_0/(2\pi) > 0$ is the carrier frequency, β is the modulation, T is the pulse duration, and

$$I_{(0,T]}(t) = \begin{cases} 1 & \text{if } t \in (0, T] \\ 0 & \text{otherwise} \end{cases}.$$

We denote the wave speed by c, and define the round trip delay between $(x_0, 0, h_0)$ and $(x, y, 0)$ by

$$\tilde{\tau}(x, y; x_0) := \frac{2}{c}\sqrt{(x - x_0)^2 + y^2 + h_0^2}. \tag{2}$$

Let E_{x_0} be the irradiated area in xy-plain when the satellite is at the point $(x_0, 0, h_0)$. Then, since the wave speed is much faster than the satellite's, at time t, the satellite receives the returned signal from each point $(x, y) \in E_{x_0}$ in the form

$$A(x, y)s(t - \tilde{\tau}(x, y; x_0)).$$

The received signal at time t is the mixture of the return from all $(x, y) \in E_{x_0}$, so that we have an expression of the received signal at t:

$$H(x_0, t) = \iint_{E_{x_0}} A(x, y)s(t - \tilde{\tau}(x, y, x_0))\, dxdy. \tag{3}$$

Remark 1 Consider the case where $A(x, y)$ has the form

$$A(x, y) = \sum_{k=1}^{m} \rho_k\, \delta(x - x_k, y - y_k) \tag{4}$$

in particular, where $\rho_k > 0,\ k = 1, 2, \ldots, m$, are constants and

$$\delta(x, y) = \begin{cases} 1 & \text{if } (x, y) = (0, 0) \\ 0 & \text{otherwise} \end{cases}.$$

If we assume that

$$\int_{-\infty}^{\infty}\int_{-\infty}^{\infty}\delta(x,y)\,dxdy=1, \tag{5}$$

then (3) becomes

$$H(x_0,t)=\sum_{(x_k,y_k)\in E_{x_0}}\rho_k\,s(t-\tilde{\tau}(x_k,y_k;x_0)). \tag{6}$$

This agrees with the conventional discrete point targets model (see [1], for example). Therefore the model (3) is more general expression of the received signal.

The well-known pulse compression technique for higher resolution is based on the point targets model (6). The model is natural when we review the development of radar system. In the early days of radar, targets were in effect points such as aircraft and missiles. But the model is not necessarily appropriate if the target objects have shapes and areas, which are common in SAR. Since objects on the ground are expressed by a point or a set of points in the modeling, the information about shapes and areas is not sufficiently preserved. Such information is recovered by the post process, distortion correction, location correction, and so on. We note also that (5) holds in the sense of distribution rigorously, not in ordinal sense. Then what if we impose a condition on (3) so as to preserve the information about shapes and areas and analyze such (3) without (5)? We can expect that a method is derived in which recovering shapes and areas is possible without the post process.

To accomplish the purpose, we introduce a local polar coordinate system

$$\begin{cases} x=r\sin\theta+x_0\\ y=r\cos\theta \end{cases} \tag{7}$$

with the domain

$$E=\{(r,\theta):r_1\le r\le r_2,\ |\theta|\le\theta_0\}.$$

The interval $[r_1,\,r_2]$ denotes the scan range and $\theta_0\in(0,\pi/2)$ gives the scan angle. The angle of $(x,y,0)$ under the local coordinate system (7) is defined by $\theta\in(-\pi/2,\pi/2)$ satisfying

$$\cos\theta=\frac{y}{\sqrt{(x-x_0)^2+y^2}}$$

together with $\theta>0$ if $x>x_0$ and $\theta<0$ if $x<x_0$ (see Figure 2).

(Figure 2: Local polar coordinate system)

The coordinate system (7) makes it possible to rewrite $\tilde{\tau}$ as a function of r only,

$$\begin{aligned}\tilde{\tau}(x,y;x_0) &= \frac{2}{c}\sqrt{(x-x_0)^2+y^2+h_0^2}\\ &= \frac{2}{c}\sqrt{r^2+h_0^2}=:\tau(r).\end{aligned}$$

So hence

$$\begin{aligned}H(x_0,t) &= \iint_E A(r\sin\theta+x_0,r\cos\theta)\,s(t-\tau(r))\left|\frac{\partial(x,y)}{\partial(r,\theta)}\right|d\theta dr\\ &= \int_{r_1}^{r_2}\left(\int_{-\theta_0}^{\theta_0}A(r\sin\theta+x_0,r\cos\theta)\,d\theta\right)s\left(t-\tau(r)\right)\,r\,dr.\end{aligned} \tag{8}$$

The argument below is based on this representation.

The coordinate system (7) is the key to derive our reconstruction method in the next section. Reconstructing the reflection coefficient is nothing but extracting the integrand $A(x,y)$ from the integral $H(x_0,t)$. Then it is reasonable to calculate the difference of the integral, and the operators composing our method is essentially defined by the differences in r-direction and θ-direction. The coordinate system (7) simplifies the calculation since it changes the irradiated area E_{x_0} into the rectangle E of (r,θ). It is intuitively natural as well since the irradiated area can be well approximated by a sector.

We impose a condition about the reflection coefficient as Condition A:

Condition A The reflection coefficient $A(x,y)$ has the form

$$A(x,y) = \sum_{k=1}^{\infty} \rho_k \, I_{B_k}(x,y),$$

where

$$B_i \cap B_j = \emptyset \ (i \neq j), \quad \bigcup_{k=1}^{\infty} B_k = \boldsymbol{R}^2 = xy\text{−plane},$$

and the boundary ∂B_k of each B_k is parallel to x-axis or y-axis.

Remark 2 The mesh model used often satisfies Condition A. So does the reflection coefficient (4) in point target model by regarding isolated points as parallel to both x and y axes.

3 Main Results

We now state the main theoretical results. For simple description, put

$$\bar{A}(x_0,r) = \int_{-\theta_0}^{\theta_0} A(r\sin\theta + x_0,\ r\cos\theta)\, d\theta,$$

then

$$H(x_0,t) = \int_{r_1}^{r_2} \bar{A}(x_0,r)\, s(t-\tau(r))\, r\, dr$$

by (8). We set $\beta = 0$ in the transmitted signal (1) since the modulation parameter β is controllable. The modulation is originally introduced to improve the resolution in the range direction. But our approach is different from the range compression so that modulating the transmitted signal is not needed. The following theorems define two kinds of operators and describe their characteristics. Theorem 1 is to extract $\bar{A}(x_0,r)$ from $H(x_0,t)$, and Theorem 2 is to calculate $A(x,y)$ approximately from $\bar{A}(x_0,r)$.

Theorem 1 Suppose that Condition A holds and the satellite is at $(x_0,0,h_0)$. Put

$$D_{\Delta t}H(x_0,t) := \frac{4}{c^2}\left\{e^{-i\omega_0\Delta t/2}H(x_0,t+\Delta t/2) - e^{i\omega_0\Delta t/2}H(x_0,t-\Delta t/2)\right\}, \quad t\in\boldsymbol{R}, \quad \Delta t>0,$$

and for every $r^*\in(r_1,r_2)$ define $t^*=\tau(r^*)$ and

$$S_{H,\Delta t}(x_0,t^*) := \frac{1}{t^*\Delta t}\sum_{k=0}^{m} D_{\Delta t}H\,(x_0,\, t^*-(m-k)T)\, e^{i(m-k)\omega_0 T}, \tag{9}$$

where m is an integral part of $(t^* - \tau(r_1))/T$. Then

$$\lim_{\Delta t \to +0} S_{H,\Delta t}(x_0, t^*)$$

$$= \begin{cases} \bar{A}(x_0,\, r^*) & \text{if } r^* \text{ is a continuous point of } \bar{A}(x_0,\, r) \\ \dfrac{1}{2}\left\{\bar{A}(x_0,\, r^* - 0) + \bar{A}(x_0,\, r^* + 0)\right\} & \text{otherwise.} \end{cases}$$

Remark 3 This theorem requires the existence of the right-side and the left-side limits $\bar{A}(x_0,\, r^* \pm 0) = \lim_{r \to r^* \pm 0} \bar{A}(x_0,\, r)$. It is ensured by Lemma in Appendix 1.

Before stating Theorem 2, we introduce some notations. Suppose that Condition A holds and a satellite is at $(x, 0, h_0)$. When $r \in [r_1, r_2]$ is fixed, a set of angles

$$\Theta(x, r) := \{\theta = \theta(x, r) : |\theta| < \theta_0,\ (r\sin\theta + x,\, r\cos\theta) \in \partial B_k \text{ for some } k\}$$

is defined (see Figure 3),

(Figure 3 : Relation between $\theta_k(x, r)$ and objects on the ground surface)

where each B_k is a set in Condition A and ∂B_k denotes the boundary of B_k. Under Condition A, if the number p of elements in $\Theta(x, r)$,

$$0 \le p = p(x, r) := \sharp\Theta(x, r),$$

is finite, then we may assume that

$$-\theta_0 < \theta_1(x, r) < \theta_2(x, r) < \cdots < \theta_{p-1}(x, r) < \theta_p(x, r) < \theta_0$$

for $\Theta(x, r) = \{\theta_k(x, r)\}_{k=1}^{p}$ (see Figure 3 again for detail). We proceed to Theorem 2.

Theorem 2 Suppose that Condition A holds. For every $x \in \boldsymbol{R}$ and $r \in [r_1, r_2]$, define

$$P_{\bar{A},\,\Delta x}(x, r) := \frac{r}{\Delta x}\{\bar{A}(x + \Delta x, r) - \bar{A}(x, r)\}$$

with $\Delta x > 0$ and

$$P_{\bar{A}}(x, r) := \lim_{\Delta x \to +0} P_{\bar{A},\,\Delta x}(x, r).$$

Let $x \in \boldsymbol{R}$ and $r \in [r_1, r_2]$ be arbitrarily given, $p = \sharp\Theta(x, r)$ be finite, and

$$A(r\sin\theta + x,\, r\cos\theta) = \begin{cases} \rho_0 & \text{if} \quad -\theta_0 < \theta < \theta_1(x, r) \\ \rho_k & \text{if} \quad \theta_k(x, r) < \theta < \theta_{k+1}(x, r), \text{ for } k = 1, 2, \ldots, p-1 \\ \rho_p & \text{if} \quad \theta_p(x, r) < \theta < \theta_0 \end{cases},$$

where $\{\rho_k\}_{k=0}^{p}$ are nonnegative constants and $\Theta(x, r) = \{\theta_k(x, r)\}_{k=1}^{p}$. Then an approximation about a difference of $A(\cdot, \cdot)$:

$$A(r\sin\theta_0 + x, r\cos\theta_0) - A(-r\sin\theta_0 + x, r\cos\theta_0) = P_{\bar{A}}(x, r) + \eta(x, r) \tag{10}$$

holds together with the evaluation of the error term

$$|\eta(x, r)| \le \frac{\theta_0^2}{2 - \theta_0^2} \sum_{k=1}^{p} |\rho_{k-1} - \rho_k|. \tag{11}$$

The reconstruction method derived by Theorem 1 and Theorem 2 is theoretically as follows. Replace $-r\sin\theta_0 + x$ and $r\cos\theta_0$ by x and y respectively in (10), and suppose that $\theta_0 > 0$ is so small that $\eta(x,r)$ is negligible in (10) by (11). Then we have

$$A(x + 2y\tan\theta_0\,, y) \simeq A(x,y) + P_{\bar{A}}\left(x + y\tan\theta_0\,,\ \frac{y}{\cos\theta_0}\right) \tag{12}$$

for $(x,y) \in [0,\infty)\times[r_1\cos\theta_0\,, r_2\cos\theta_0]$. This can be regarded as an update formula of $A(\cdot,\cdot)$ by $P_{\bar{A}}(\cdot,\cdot)$. The values $\{P_{\bar{A}}(\cdot,\cdot)\}$ are calculated from observations in the following manner. Suppose that continuous received signal $\{H(x,t) : x \geq 0,\ \tau(r_1) \leq t \leq \tau(r_2)\}$ is observed.

The first thing, apply $D_{\Delta t}$ to $H(x,t)$ and calculate $S_{H,\Delta t}(x,t)$, then we have a set

$$\{\bar{A}(x,r) : x \geq 0,\ r_1 < r < r_2\} = \{\bar{A}(x,\ \tau^{-1}(t)) : x \geq 0,\ \tau(r_1) < t < \tau(r_2)\} \tag{13}$$

by $\bar{A}(x,r) = \lim_{\Delta t\to+0} S_{H,\Delta t}(x,t)$ as long as $r = \tau(t)$ is a continuous point of $\bar{A}(x,r)$. Assuming that the set (13) is obtained correctly for all r, we then obtain a set

$$\left\{P_{\bar{A}}\left(x,\ \frac{y}{\cos\theta_0}\right) : x \geq 0,\ r_1\cos\theta_0 < y < r_2\cos\theta_0\right\} = \{P_{\bar{A}}(x,r) : x \geq 0,\ r_1 < r < r_2\} \tag{14}$$

by applying the operator $P_{\bar{A},\Delta x}$ to $\bar{A}$ and take the limit $P_{\bar{A}}(x,r) = \lim_{\Delta x\to+0} P_{\bar{A},\Delta x}(x,r)$.

Suppose also that the initial value set R_0 of $A(x,y)$ is given by

$$R_0 := \{A(x,y) : 0 \leq x \leq 2y\tan\theta_0,\ r_1\cos\theta_0 \leq y \leq r_2\cos\theta_0\}, \tag{15}$$

and let $y \in [r_1\cos\theta_0,\ r_2\cos\theta_0]$ be fixed. Then it follows from (12) and (15) that a set of reconstruction results $\widehat{A}(x,y)$ of $A(x,y)$,

$$R(y,1) := \{\widehat{A}(x,y) : 2y\tan\theta_0 \leq x \leq 4y\tan\theta_0\},$$

is obtained. Similarly, the iterative use of the update formula (12) yields that

$$R(y,k) := \{\widehat{A}(x,y) : 2ky\tan\theta_0 \leq x \leq 2(k+1)y\tan\theta_0\}, \quad k = 1,2,\ldots,$$

subsequently. Considering this procedure for all $y \in [r_1\cos\theta_0,\ r_2\cos\theta_0]$, we finally have the whole reconstruction result

$$\left(\bigcup_y\bigcup_k R(y,k)\right)\bigcup R_0 = \{\widehat{A}(x,y) : x \geq 0,\ r_1\cos\theta_0 \leq y \leq r_2\cos\theta_0\}.$$

In practice, however, the continuous observation cannot be obtained, neither can the limits $\lim_{\Delta t\to+0} S_{H,\Delta t}(t,x)$ and $\lim_{\Delta x\to+0} P_{\bar{A},\Delta x}$. Therefore the observations should be discrete, and the calculation of the limits has to be replaced by approximations with Δt and Δx fixed sufficiently small. Numerical examples using such approximations are given in Section 4.

In the pulse compression technique, the reflection coefficient $A(x,y)$ is discretized by point targets and the information of each target is recovered by using sinc function. Point targets are isolated points and they are regarded as singular points. Then we can say that the mathematical interpretation of the pulse compression technique is gathering the information about $A(x,y)$ in the singular point of $A(x,y)$ by Dirichlet kernel. On the other hand, our method focuses on extracting $A(x,y)$ from $H(x,t)$ in the continuous points

(regular points) of $A(x,y)$. Discontinuous points (singular points) of $A(x,y)$ cause discontinuity of $\bar{A}(x,r)$ with respect to r (see the proof of Lemma in Appendix 1), and as seen in Theorem 1, extracting $\bar{A}(x,r)$ correctly in the discontinuous points is rather difficult.

4 Numerical Examples

4.1 Fixed Increments Approximation

As mentioned in the previous section, we fix the increment Δt and Δx sufficiently small and substitute $S_{H,\Delta t}$ and $P_{\bar{A},\Delta x}$ for these limits as $\Delta t,\, \Delta x \to +0$ when we apply our method in practice.

Based on Theorem 1, Theorem 2 and (12), choose Δt and Δx so small that the following approximations hold:

$$\begin{aligned} & A(x+2y\tan\theta_0,\, y) \\ & \simeq \quad A(x,y) + P_{\bar{A},\Delta x}\left(x+2y\tan\theta_0,\, \frac{y}{\cos\theta_0}\right) \\ & = \quad A(x,y) \\ & \qquad + \frac{1}{\Delta x}\cdot\frac{y}{\cos\theta_0}\left\{\bar{A}\left(x+\Delta x+2y\tan\theta_0,\, \frac{y}{\cos\theta_0}\right) - \bar{A}\left(x+2y\tan\theta_0,\, \frac{y}{\cos\theta_0}\right)\right\}, \end{aligned} \tag{16}$$

$$\bar{A}(x,r) \simeq S_{H,\Delta t}(x,t), \quad r=\tau^{-1}(t). \tag{17}$$

Rigorously the last approximation holds if $r = y/\cos\theta_0$ is a continuous point of $\bar{A}(x+\Delta x+2y\tan\theta_0,\, r)$ and $\bar{A}(x+2y\tan\theta_0,\, r)$ in the light of Theorem 1 . For fixed Δt and Δx, where Δt is chosen so that $T/\Delta t$ is an integer, suppose that sufficient amount of discrete observations

$$\{H(x_i,t_{ij}) : x_i \geq 0,\, \tau(r_1) \leq t_{ij} \leq \tau(r_2),\, x_{i+1}-x_i = \Delta x,\, t_{ij+1}-t_{ij} = \Delta t\}$$

are obtained to calculate $S_{H,\Delta t}(x_i,t_{ij})$ in (17). Then $\{\bar{A}(x_i,r_{ij}) : r_{ij} = \tau^{-1}(t_{ij})\}$ is derived and thus the reconstruction results $\{\widehat{A}(x_i,y_{ij})\}$ as an approximation of $\{A(x_i,y_{ij})\}$ are subsequently obtained by (16).

We now show some numerical examples to observe the reconstruction results in our proposing method and make comparison with the pulse compression technique. In this subsection, we deal with noiseless cases to see the characteristic of the method itself.

The first thing we consider the case where the reflection coefficient $A(x,y)$ has the form

$$A(x,y) = \begin{cases} 1 & \text{if } x \in (14999, 15001) \text{ and } y \in (399999, 400001) \\ 1 & \text{if } x \in (14999, 15001) \text{ and } y \in (400009, 400011) \\ 0 & \text{otherwise} \end{cases} \tag{18}$$

in accordance with Condition A. This correspond with the situation that there are two 2[m] $\times$ 2[m] size square objects on a range-direction line 10[m] distance apart with respect to their centers. In the application of the pulse compression, $A(x,y)$ has to be modeled in the form (4) as point targets. Since the objects are small, we express each object as a point. Then

$$A(x,y) = \delta(15000,\, 400000) + \delta(15000,\, 400010) \tag{19}$$

is assumed for the pulse compression. The parameters of the radar are taken from the satellite JERS-1 operated practically from 1992 to 1998 (see Appendix 4 for detail). In this case, $\theta_0 \simeq 1.707 \times 10^{-2}$ and the upper bound of the error term $\eta(x, r)$ in (11) becomes $1.457 \times 10^{-4} \times \sum_k |\rho_{k-1} - \rho_k|$. Hence the error term is negligible if the variation of $\{\rho_k\}$ is not so large.

(Figure 4: Ground image reconstructed by the pulse compression) (Figure 5: Ground image reconstructed by our method)

One pixel has 1[m] × 1[m] size in both figures. Figure 4 is the reconstruction result from the pulse compression technique, which consists of the range compression, the azimuth compression and three-multilook processing. Figure 5 is that from our method, where the increments are set $\Delta t = 30\pi/\omega_0$[m] and $\Delta x = 3$[m], and we assume that $A(x, y) \equiv 0$ on the initial value set R_0 because of (18). There seems to be only one target object in Figure 4 since the pulse compression cannot separate the echoes from the two target points. In fact, the highest resolution of SAR system in JERS-1 was 18[m]. Therefore it is hard task to discriminate two objects 10[m] distance apart. In our method, Δt and Δx set as above give 3[m] resolution at the highest. Then we can see clearly in Figure 5 that there are two objects apart on the ground.

We show a little complicated example. Suppose that $A(x, y)$ is given by

$$A(x,y) = \begin{cases} 1 & \text{if } x \in (14999, 15001) \text{ and } y \in (399995, 400005) \\ 1 & \text{if } x \in (15008, 15015) \text{ and } y \in (399999, 400001) \\ 0 & \text{otherwise} \end{cases} . \tag{20}$$

This means that there are two rectangular objects. One is long along x-axis and the other is along y-axis. Similarly to (19), the reflection coefficient (20) must be reformulated in terms of point targets. Since the objects are rectangles, we represent them by two points respectively. Hence we replace (20) by

$$A(x,y) = \{\delta(15000, 399997) + \delta(15000, 400003)\} + \{\delta(15009, 400000) + \delta(15014, 400000)\}$$

for the pulse compression.

(Figure 6: the pulse compression) (Figure 7: our method)

Figure 6 is obtained by the pulse compression and Figure 7 is obtained by our method with $A(x, y) \equiv 0$ on R_0. Figure 7 implies that a marked characteristic of our method is shape recovery as well as reflection coefficient reconstruction. It is impossible to recognize the shape in Figure 6. We note that any corrections as the post process, such as distortion correction and location correction, are not made to obtain Figure 7 (and Figure 5 also). This difference from the pulse compression technique comes from how to model the reflection coefficient $A(x, y)$ at the beginning. Once the point targets model is assumed to apply the pulse compression, the reflection coefficient is discretized by a set of isolated points. Then the model fails to preserve the information about shapes and areas of objects in rigorous sense. Therefore correction works are indispensable in the post process to recover the dropped information. By contrast, Condition A on which our method is based does not require discretization of the reflection coefficient, so that the information about shapes and areas are preserved in the model (8). Thus our method derived from (8) makes it possible to recover the shapes and areas without correction works afterwards if Δt and Δx are sufficiently small.

4.2 Sensitivity to Noise

We consider the problem of the sensitivity to noise in this subsection. Suppose that the received signal $H(x_0,t)$ is contaminated by random additive noise $\varepsilon(x_0,t)$,

$$G(x_0,t) := H(x_0,t) + \sigma\,\varepsilon(x_0,t),$$

where $\sigma > 0$ is the noise level (standard deviation) and we suppose that $E[\varepsilon(x_0,t)] = 0$ and $\mathrm{Var}[\varepsilon(x_0,t)] = E[\{\varepsilon(x_0,t)\}^2] = 1$ for all (x_0,t).

The pulse compression technique is robust against additive noise. In the case of the range compression, for example, the received signal $G(x_0,t)$ is transformed by the matched filter $h(t) = \exp(-i\beta t^2) I_{[0,T)}(t)$ as

$$\begin{aligned}\frac{1}{T}(G*h)(t) &= \frac{1}{T}(H*h)(t) + \frac{\sigma}{T}(\varepsilon*h)(t)\\ &\simeq \exp\{i\omega_0(t-\tilde\tau)\}\,\frac{\sin\{\beta T(t-\tilde\tau)\}}{\beta T(t-\tilde\tau)}\,I_{(\tilde\tau+T/2,\,\tilde\tau+3T/2]}(t)\\ &\quad + \frac{\sigma}{T}\int_0^T \varepsilon(x_0,u)h(t-u)\,du, \qquad (21)\end{aligned}$$

where $\tilde\tau = \tilde\tau(x,y,;x_0)$ is the round trip delay (2) and the symbol "$*$" denotes convolution. The approximation in (21) holds when $|\beta|T^2$ is sufficiently large. Then we have

$$\begin{aligned}&\left(E\left[\left|\frac{\sigma}{T}\int_0^T \varepsilon(x_0,u)h(t-u)\,du\right|^2\right]\right)^{1/2}\\ &\le \frac{\sigma}{T}\left(\int_0^T\int_0^T E[|\varepsilon(x_0,u)\,\varepsilon(x_0,v)|]\,|h(t-u)h(t-v)|\,dudv\right)^{1/2} \le \frac{\sigma}{T}\cdot T = \sigma, \qquad (22)\end{aligned}$$

which means the noise level is less than or equal to the original one. The same holds true in the azimuth compression. Then the upper bound can be reduced to $\sigma/\sqrt{n}$ at the sacrifice of the resolution a little if the SAR adopts n-multilook system.

On the other hand, our proposing method essentially consists of difference-based operators. Difference calculations are deficient in the robustness against additive noise in general, and it holds true for our method unfortunately. Suppose that each $\varepsilon(x_0,t)$ is independently and identically distributed in accordance with a probability distribution with mean zero and variance one, and calculate $S_{H,\Delta t}(x_0,t^*)$ of (9) replaced by $G(x_0,t)$:

$$\begin{aligned}S_{H,\Delta t}(x_0,t^*) &= \frac{1}{t^*\Delta t}\sum_{k=0}^{m} D_{\Delta t}\,H(x_0,\,t^*-(m-k)T)\,e^{i(m-k)\omega_0 T}\\ &\quad + \frac{\sigma}{t^*\Delta t}\sum_{k=0}^{m} D_{\Delta t}\,\varepsilon(x_0,\,t^*-(m-k)T)\,e^{i(m-k)\omega_0 T}. \qquad (23)\end{aligned}$$

Then the noise level of the second term in the right-hand side becomes

$$\left(E\left[\left|\frac{\sigma}{t^*\Delta t}\sum_{k=0}^{m} D_{\Delta t}\,\varepsilon(x_0,\,t^*-(m-k)T)\,e^{i(m-k)\omega_0 T}\right|^2\right]\right)^{1/2} = \frac{4\sqrt{2(m+1)}\,\sigma}{c^2\,t^*\Delta t}.$$

Therefore, when we apply (16), the upper bound of the noise level is finally given by

$$\left(\frac{4\sqrt{2\left(\lfloor (\tau(r_2)-\tau(r_1))/T \rfloor + 1\right)}}{c^2\,\tau(r_2)\,\Delta t} \right) \left(\frac{2\,r_2}{\Delta x} \right) \sigma, \tag{24}$$

where $\lfloor \alpha \rfloor$ is an integral part of α. This bound diverges to infinity as Δt or Δx tends to zero though the resolution becomes higher in that case. We face the trade-off relation between the resolution and the noise level analogously to the multilook noise reduction method.

In the practical use, however, the increments Δt and Δx are chosen sufficiently small and fixed. Then the bound (24) is useful to determine the appropriate resolution by taking the influence of the noise into account. Using the JERS-1 parameters, for instance, we can further rewrite (24) into

$$\frac{3.444 \times 10^{-8}}{\Delta t\,\Delta x}\sigma. \tag{25}$$

Set $\Delta t = 30\pi/\omega_0$[s] and $\Delta x = 3$[m] in the same way as Subsection 4.1, then the resolution is 3[m] and the upper bound (25) becomes $0.9758 \times \sigma$. The three-multilook system adopted in JERS-1 can reduce the noise level to smaller $0.5774 \times \sigma$. But the resolution of JERS-1 is six times larger 18[m], and the upper bound of the noise level in our method does not increase at least as long as we fix 3[m] resolution. The upper bound (24) implies also that the flexible adjustment between the resolution and the noise level is possible since Δt and Δx are both continuous variables, whereas the adjustment is made in the unit of look numbers only in the n-multilook system.

We show a numerical example of randomly contaminated case and compare the result with that of pulse compression. Suppose that the reflection coefficient $A(x, y)$ has the form (18) and the corresponding point target model is (19). The parameters and the increments are also the same as those in Subsection 4.1.

(Figure 8: the pulse compression) (Figure 9: our method)

Figure 8 and Figure 9 are the reconstruction results in the case of the noise level $\sigma = 0.3$. The former is the result from the pulse compression and the latter is that from our method. One pixel has 1[m] $\times$ 1[m] size in the both figures, and it is assumed that each $\varepsilon(x_0, t)$ is independent and has the standard normal distribution $N(0, 1)$ for simplicity.

Observing Figure 9, we know that there are two objects apart and they have long shape furthermore. The pulse compression technique can detect the two objects also according to Figure 8. The comparison of Figure 8 with Figure 6 proves that the pulse compression technique is robust against additive random noise since both figures are almost the same. The three-multilook system seems to work well to reduce the noise level. But the shape of the objects is not clear. Thus, as long as the examples above, our method gives better reconstruction results, shape recovery and clear image, than the pulse compression does in the case contaminated by random additive noise, too.

5 Concluding Remarks

We proposed a new difference-based method to reconstruct the reflection coefficient of the ground surface. The essential difference between our method and the conventional pulse compression technique is how to

model the reflection coefficient $A(x, y)$. We are interested in target objects having shapes and areas on the ground. So that it is necessary to model the reflection coefficient so as to preserve that kind of information. Then our method derived from such modeling makes it possible to recover shapes and areas without post-correction works if the increment Δt and Δx are sufficiently small. The figures in Subsection 4.1 prove that. Thus reconstruction process becomes simple since we have only to calculate the difference of the received signal in essence.

Generally speaking, difference-based method is deficient in the robustness against additive noise. Sampling in small interval and difference calculation cause the increase of the noise level. Unfortunately our method is not free from the rule. But as shown in Subsection 4.2, the upper bound of the noise level can be small by adjusting the resolution. The figures in Subsection 4.2 show in effect that our method still performs shape recovery with higher resolution than the pulse compression technique even in the case contaminated randomly by white noise. We note also that our method is not an edge detector though it consists of the difference-based operators. Our difference calculation is not for edge detection but for extracting the integrand $A(x, y)$ from the multiple integral $H(x, t)$ with respect to the continuous points of $A(x, y)$. That seems to be one of the reasons why our method is not so influenced by additive noise.

In the analysis of SAR signal, eliminating the multiplicative speckle noise is an important problem ([4], [5], [9], [10], for example). The papers discussing this problem are based on point targets model and probability distributions of noise are assigned to each target point. But, as we stated repeatedly, the reflection coefficient is not discretized in our model to preserve the information about shapes and areas, so that how to assign the probability distribution of multiplicative noise is completely different and it must be deeply studied from scratch. Then this problem in our method is left for further research.

Appendices

Appendix 1 : Preliminary Lemma

The following lemma ensures the statement of Theorem 1 holds.

Lemma Let x_0 be arbitrarily fixed. Then for every $r^* \in [r_1, r_2]$, both the right-side and the left-side limits

$$\bar{A}(x_0,\, r^* \pm 0) = \lim_{r \to r^* \pm 0} \bar{A}(x_0,\, r)$$

exist and they are finite, provided that only the right-side or the left-side limit is considered when $r^* = r_1$ or $r^* = r_2$.

Proof. For every $\theta \in [-\theta_0, \theta_0]$, Condition A yields that the limits

$$\lim_{r \to r^* \pm 0} A(r \sin\theta + x_0, r\cos\theta) =: a^{\pm}(\theta; r^*)$$

exist for every $r^* \in [r_1, r_2]$, Then it follows from bounded convergence theorem that

$$0 \le \lim_{r \to r^* \pm 0} \bar{A}(x_0, r) = \lim_{r \to r^* \pm 0} \int_{-\theta_0}^{\theta_0} A(r\sin\theta + x_0, r\cos\theta)\, d\theta = \int_{-\theta_0}^{\theta_0} a^{\pm}(\theta; r^*)\, d\theta < \infty.$$

∎

Appendix 2 : Proof of Theorem 1

The first thing we rewrite (3) for simple description. Let $u = \tau(r)$, $t_k = \tau(r_k)$, $k = 1, 2$, and $\xi(u) = \tau^{-1}(u)$, then

$$\begin{aligned} H(x_0, t) &= \int_{t_1}^{t_2} \bar{A}(x_0, \xi(u))\, s(t-u)\, \xi(u)\, \xi'(u)\, du \\ &= \frac{c^2}{4} \int_{-\infty}^{\infty} \bar{A}(x_0, \xi(u))\ \exp\{i\omega_0(t-u)\}\, I_{(t-T,\, t)\cap(t_1,\, t_2)}(u)\, u\, du, \end{aligned} \tag{26}$$

where we have used in the second equality that $\xi(u)\,\xi'(u) = c^2 u/4$ derived from

$$\xi(u) = \frac{c}{2}\left(u^2 - \frac{4h_0^2}{c^2}\right)^{1/2} \quad \text{and} \quad \xi'(u) = \frac{cu}{2}\left(u^2 - \frac{4h_0^2}{c^2}\right)^{-1/2}.$$

For every $\Delta t > 0$, the representation (26) yields that

$$\begin{aligned} &\frac{4}{c^2}\, e^{\mp i\omega_0 \Delta t/2} H(x_0,\, t \pm \Delta t/2) \\ &= e^{\mp i\omega_0 \Delta t/2} \int_{-\infty}^{\infty} \bar{A}(x_0, \xi(u)) \exp\{i\omega_0(t \pm \Delta t/2 - u)\}\, u\, I_{(t-T\pm\Delta t/2,\, t\pm\Delta t/2)\cap(t_1,\, t_2)}(u)\, du \\ &= \int_{-\infty}^{\infty} \bar{A}(x_0, \xi(u)) \exp\{i\omega_0(t-u)\}\, u\, I_{(t-T\pm\Delta t/2,\, t\pm\Delta t/2)\cap(t_1,\, t_2)}(u)\, du. \end{aligned} \tag{27}$$

Letting $\Delta t \to 0$ later, we may assume that $0 < \Delta t < T$. Then it follows from (27) that

$$\begin{aligned} D_{\Delta t} H(x_0, t) &= \frac{4}{c^2}\left\{e^{-i\omega_0 \Delta t/2} H(x_0,\, t + \Delta t/2) - e^{i\omega_0 \Delta t/2} H(x_0,\, t - \Delta t/2)\right\} \\ &= \int_{-\infty}^{\infty} \bar{A}(x_0, \xi(u)) \exp\{i\omega_0(t-u)\}\ u\, I_{(t-\Delta t/2,\, t+\Delta t/2)\cap(t_1,\, t_2)}(u)\, du \\ &\quad - \int_{-\infty}^{\infty} \bar{A}(x_0, \xi(u)) \exp\{i\omega_0(t-u)\}\ u\, I_{(t-T-\Delta t/2,\, t-T+\Delta t/2)\cap(t_1,\, t_2)}(u)\, du. \end{aligned} \tag{28}$$

Let $r^* \in (r_1, r_2)$ be given and $m \geq 0$ be the integer satisfying $t_1 + mT \leq t^* < t_1 + (m+1)T$. Then, for $t^* = \tau(r^*)$ and every $k = 0, 1, \ldots, m$, the equation (28) gives that

$$\begin{aligned} &D_{\Delta t} H\,(t^* - (m-k)T, x_0) \\ &= e^{-i\omega_0(m-k)T} \left\{ \int_{-\infty}^{\infty} \bar{A}(x_0, \xi(u)) \exp\{i\omega_0(t^* - u)\}\, u\, I_{(t^*-(m-k)T-\Delta t/2,\, t^*-(m-k)T+\Delta t/2)\cap(t_1,\, t_2)}(u)\, du \right. \\ &\quad \left. - \int_{-\infty}^{\infty} \bar{A}(x_0, \xi(u)) \exp\{i\omega_0(t^* - u)\}\, u\, I_{(t^*-(m-k+1)T-\Delta t/2,\, t^*-(m-k+1)T+\Delta t/2)\cap(t_1,\, t_2)}(u)\, du \right\}. \end{aligned} \tag{29}$$

Therefore, by choosing $\Delta t \in (0, T)$ so small that $(t^* - \Delta t/2,\, t^* + \Delta t/2) \subset (t_1, t_2)$,

$$\sum_{k=0}^{m} D_{\Delta t} H\,(t^* - (m-k)T, x_0)\, e^{i(m-k)\omega_0 T}$$

$$= \int_{-\infty}^{\infty} \bar{A}\left(x_0, \xi(u)\right) \exp\left\{i\omega_0\left(t^* - u\right)\right\} u\, I_{(t^*-\Delta t/2,\, t^*+\Delta t/2)\cap(t_1,\, t_2)}(u)\, du$$

$$- \int_{-\infty}^{\infty} \bar{A}\left(x_0, \xi(u)\right) \exp\left\{i\omega_0\left(t^* - u\right)\right\} u\, I_{(t^*-(m+1)T-\Delta t/2,\, t^*-(m+1)T+\Delta t/2)\cap(t_1,\, t_2)}(u)\, du$$

$$= \int_{t^*-\Delta t/2}^{t^*+\Delta t/2} \bar{A}\left(x_0, \xi(u)\right) \exp\left\{i\omega_0\left(t^* - u\right)\right\} u\, du$$

$$- \int_{-\infty}^{\infty} \bar{A}\left(x_0, \xi(u)\right) \exp\left\{i\omega_0\left(t^* - u\right)\right\} u\, I_{(t_1,\, t_1+\Delta-T+\Delta t/2)\cap(t_1,\, t_2)}(u)\, du, \tag{30}$$

where $\Delta \in [0, T)$ is the residual $\Delta = t^* - t_1 - mT$. When we choose Δt to be less than or equal to $2(T-\Delta)$ in addition to $\Delta t \in (0, T)$, the second integral on the right hand side of (30) vanishes. Thus

$$S_{H,\Delta t}(x_0, t^*) = \frac{1}{t^*\Delta t} \sum_{k=0}^{m} D_{\Delta t} H\left(t^* - (k-m)T, x_0\right) e^{i(m-k)\omega_0 T}$$

$$= \frac{1}{t^*\Delta t} \int_{t^*-\Delta t/2}^{t^*+\Delta t/2} \bar{A}\left(x_0, \xi(u)\right) \exp\left\{i\omega_0\left(t^* - u\right)\right\} u\, du. \tag{31}$$

If r^* is a continuous point of $\bar{A}(x_0, r)$, then (31) yields that

$$\lim_{\Delta t \to +0} S_{H,\Delta t}(x_0, t^*) = \bar{A}(x_0, \xi(t^*)) = \bar{A}(x_0, r^*)$$

since $\xi(u)$ is a continuous function and $r^* = \tau^{-1}(t^*) = \xi(t^*)$. Suppose contrarily that r^* is a discontinuous point of $\bar{A}(x_0, r)$. Then, writing the right-hand side of (31) as

$$\frac{1}{t^*\Delta t}\left\{\int_{t^*-\Delta t/2}^{t^*} \bar{A}\left(x_0, \xi(u)\right) \exp\left\{i\omega_0\left(t^* - u\right)\right\} u du \right.$$

$$\left. + \int_{t^*}^{t^*+\Delta t/2} \bar{A}\left(x_0, \xi(u)\right) \exp\left\{i\omega_0\left(t^* - u\right)\right\} u du \right\}$$

and noting that $\xi(u)$ is monotone increasing, we obtain

$$\lim_{\Delta t \to +0} S_{H,\Delta t}(x_0, t^*) = \frac{1}{2}\left\{\bar{A}(x_0, \xi(t^* - 0)) + \bar{A}(x_0, \xi(t^* + 0))\right\}$$

$$= \frac{1}{2}\left\{\bar{A}(x_0,\, r^* - 0) + \bar{A}(x_0,\, r^* + 0)\right\}.$$

This completes the proof of Theorem 1. ∎

Appendix 3 : Proof of Theorem 2

Suppose that Condition A is satisfied. Then for given $\Theta(x, r) = \{\theta_k(x, r)\}_{k=1}^{p}$ and sufficiently small $\Delta x > 0$, there exists $\{\theta_k(x + \Delta x, r) : |\theta_k(x + \Delta x, r)| < \theta_0,\ k = 1, 2, \ldots, p\}$ such that

$$r \sin\theta_k(x, r) + x = r \sin\theta_k(x + \Delta x, r) + x + \Delta x =: x_k, \quad k = 1, 2, \ldots, p, \tag{32}$$

and

$$
\begin{aligned}
& P_{\bar{A},\Delta x}(x,r) \\
&= \frac{r}{\Delta x}\{\bar{A}(x+\Delta x,r)-\bar{A}(x,r)\} \\
&= \frac{r}{\Delta x}\left\{\left(\int_{-\theta_0}^{\theta_1(x+\Delta x,\,r)}+\sum_{k=1}^{p-1}\int_{\theta_k(x+\Delta x,\,r)}^{\theta_{k+1}(x+\Delta x,\,r)}+\int_{\theta_p(x+\Delta x,\,r)}^{\theta_0}\right)A(r\sin\theta+x,\,r\cos\theta)\,d\theta\right. \\
&\qquad\left.-\left(\int_{-\theta_0}^{\theta_1(x,\,r)}+\sum_{k=1}^{p-1}\int_{\theta_k(x,\,r)}^{\theta_{k+1}(x,\,r)}+\int_{\theta_p(x,\,r)}^{\theta_0}\right)A(r\sin\theta+x,\,r\cos\theta)\,d\theta\right\} \\
&= \frac{r}{\Delta x}\left\{\left(\rho_0\int_{-\theta_0}^{\theta_1(x+\Delta x,\,r)}d\theta+\sum_{k=1}^{p-1}\rho_k\int_{\theta_k(x+\Delta x,\,r)}^{\theta_{k+1}(x+\Delta x,\,r)}d\theta+\rho_p\int_{\theta_p(x+\Delta x,\,r)}^{\theta_0}d\theta\right)\right. \\
&\qquad\left.-\left(\rho_0\int_{-\theta_0}^{\theta_1(x,\,r)}d\theta+\sum_{k=1}^{p-1}\rho_k\int_{\theta_k(x,\,r)}^{\theta_{k+1}(x,\,r)}d\theta+\rho_p\int_{\theta_p(x,\,r)}^{\theta_0}d\theta\right)\right\} \\
&= \frac{r}{\Delta x}\left[\,\rho_0\{\theta_1(x+\Delta x,r)-\theta_1(x,r)\}-\rho_p\{\theta_p(x+\Delta x,r)-\theta_p(x,r)\}\right. \\
&\qquad\left.+\sum_{k=1}^{p-1}\rho_k\{(\theta_{k+1}(x+\Delta x,r)-\theta_{k+1}(x,r))-(\theta_k(x+\Delta x,r)-\theta_k(x,r))\}\right] \\
&= \frac{r}{\Delta x}\sum_{k=1}^{p}(\rho_{k-1}-\rho_k)\{\theta_k(x+\Delta x,r)-\theta_k(x,r))\}. \qquad (33)
\end{aligned}
$$

It follows from (32) and mean value theorem that

$$
\begin{aligned}
\frac{r}{\Delta x}\{\theta_k(x+\Delta x,r)-\theta_k(x,r)\} &= \frac{r}{\Delta x}\left\{\arcsin\frac{x_k-x-\Delta x}{r}-\arcsin\frac{x_k-x}{r}\right\} \\
&= -\left\{1-\left(\frac{x_k-x-\xi_k}{r}\right)^2\right\}^{-1/2} \qquad (0<\xi_k<\Delta x) \\
&\to -\left\{1-\left(\frac{x_k-x}{r}\right)^2\right\}^{-1/2}=-\frac{1}{\cos\theta_k(x,r)} \qquad (34)
\end{aligned}
$$

as $\Delta x\to+0$ for all $k=1,2,\ldots,p$. Combining (33) and (34), we obtain

$$
P_{\bar{A}}(x,r)=\lim_{\Delta x\to+0}P_{\bar{A},\Delta x}(x,r)=\sum_{k=1}^{p}\frac{\rho_k-\rho_{k-1}}{\cos\theta_k(x,r)}. \qquad (35)
$$

By taking it into account that

$$
A(r\sin\theta_0+x,\,r\cos\theta_0)-A(r\sin(-\theta_0)+x,\,r\cos\theta_0)=\rho_p-\rho_0=\sum_{k=1}^{p}(\rho_k-\rho_{k-1}),
$$

the equation (35) yields that

$$\begin{aligned} |\eta(x,r)| &= |\{A(r\sin\theta_0 + x,\, r\cos\theta_0) - A(-r\sin\theta_0 + x,\, r\cos\theta_0)\} - P_{\bar{A}}(x,r)| \\ &= \left|\sum_{k=1}^{p}(\rho_k - \rho_{k-1})\left(1 - \frac{1}{\cos\theta_k(r,x)}\right)\right| \leq \left(\frac{1}{\cos\theta_0} - 1\right)\sum_{k=1}^{p}|\rho_k - \rho_{k-1}| \\ &\leq \frac{\theta_0^2}{2-\theta_0^2}\sum_{k=1}^{p}|\rho_k - \rho_{k-1}|, \end{aligned}$$

where we have used that $\sup_{1\leq k\leq p}|\theta_k(x,r)| < \theta_0 < \pi/2$ in the first inequality and $\cos\theta_0 \geq 1-\theta_0^2/2$ in the second inequality. Thus the proof of Theorem 2 has been completed. ∎

Appendix 4 : JERS-1

JERS-1 (Japanese Earth Resources Satellite-1) is the satellite launched and operated by former National Space Development Agency of Japan (reorganized as Japan Aerospace Exploration Agency in 2003) from 1992 to 1998. The mission was to conduct national agricultural and forestry surveys and also to prevent people from possible natural disasters. It carried two observational equipments, synthetic aperture radar optical sensor. The parameters of the SAR system are as follows:

Carrier frequency	1275 [GHz]
Pulse duration	35 [μs]
Band width	15 [MHz]
Range resolution	18[m]
Azimuth resolution	18[m] (three-multilook)
Height of the satellite	570 [km]
Speed of the satellite	7.5 [km/s]
Length of antenna	12 [m]
Swath center	400 [km]
Swath width	75 [km]

Then we have

ω_0	=	$2\pi \times 1.275 \times 10^9$ [Hz]
β	=	$-2\pi \times 4.286 \times 10^{11}$ [Hz/s]
r_1	=	3.625×10^5 [m]
r_2	=	4.375×10^5 [m]

The swath center is at 4.000×10^5[m] along the ground range, that is, $(r,\theta) = (4.000 \times 10^5, 0)$. Since the length of antenna is 12[m], the width of the swath center along azimuth direction is 1.365×10^4[m]. Therefore we may assume that

$$\theta_0 = \arctan\left(\frac{1.365 \times 10^4 \ / \ 2}{4.000 \times 10^5}\right) \simeq 1.707 \times 10^{-2}.$$

(Figure 10: Ground surface area irradiated by radar beam)

Three-multilook system adopted by JERS-1 fixes the range and azimuth resolution at 18[m], and reduces the noise level to 0.5774 times smaller compared with single-look case (see [15] for detail).

References

[1] W. Chalin, K.Y. Liu, M. Y. Jin, Modeling and a correlation algorithm for spaceborne SAR signals, IEEE Trans. Aersp. Electron. Syst., 18(5) (1982), pp.563-575.

[2] C. E. Cook, Pulse compression -Key to more efficient radar transmission, Proc. IRE, 48. (1973), pp.310-316.

[3] J. C. Curlander, R. N. McDonough, Synthetic aperture radar : systems and signal processing, Wiley: New York, 1991.

[4] F. Gini, F. Bordoni, On the behavior of information theoretic criteria for model order selection of InSAR signals corrupted by multiplicative noise, Signal Processing, 83(5), (May 2003), pp.1047-1063.

[5] F. Gini, A. Farina, F. Lombardini, Efects of foliage on the formation of K-distributed SAR imagery, Signal Processing, 75(2), (June 1999), pp.161-171.

[6] J. R. Klauder, A. C. Price, S. Darling, W. J. Alberscheim, The theory and design of chirp radars, Bell Syst. Tech. J., 39, pp.745-808.

[7] Margaret Cheney, Mathematical Tutorial of Synthetic Aperture Radar SIAM Review, 43(2), (2001), pp.301-312.

[8] C. J. Oliver, Synthetic-aperture radar imaging, J. Phys. D, 22(7), (1989), pp.871-890.

[9] C. J. Oliver, S. Quegan, Understanding synthetic aperture radar images, Artech House, 1998.

[10] C. Salim, H. Amrane, S. Sansal, Statistical characterisation and modelling of SAR images, Signal Processing, 82(1), (2002). pp.69-92.

[11] D. Pastinaa, P. Lombardoa, A. Farinab, P. Daddia, Super-resolution of polarimetric SAR images of ship targets, Signal Processing, 83(8), (August 2003), pp.1737-1748.

[12] I.C. Sikanetaa, J. Y. Chouinard, Eigen decomposition ofthe multi-channel covariance matrix with applications to SAR-GMTI, Signal Processing, 84(9), (2002). (September 2004), pp.1501-1535.

[13] M. I. Skolnik, Radar Handbook (second edition), McGraw-Hill, 1990.

[14] C. A. Wiley, Synthetic aperture radars -a paradigm for technology evolution, IEEE Trans. Aersp. Electron. Syst., 21(3) (1989), pp.440-443.

[15] JERS-1 DATA USERS HANDBOOK, Remote Sensing Technology Center of Japan (RESTEC), 1994.

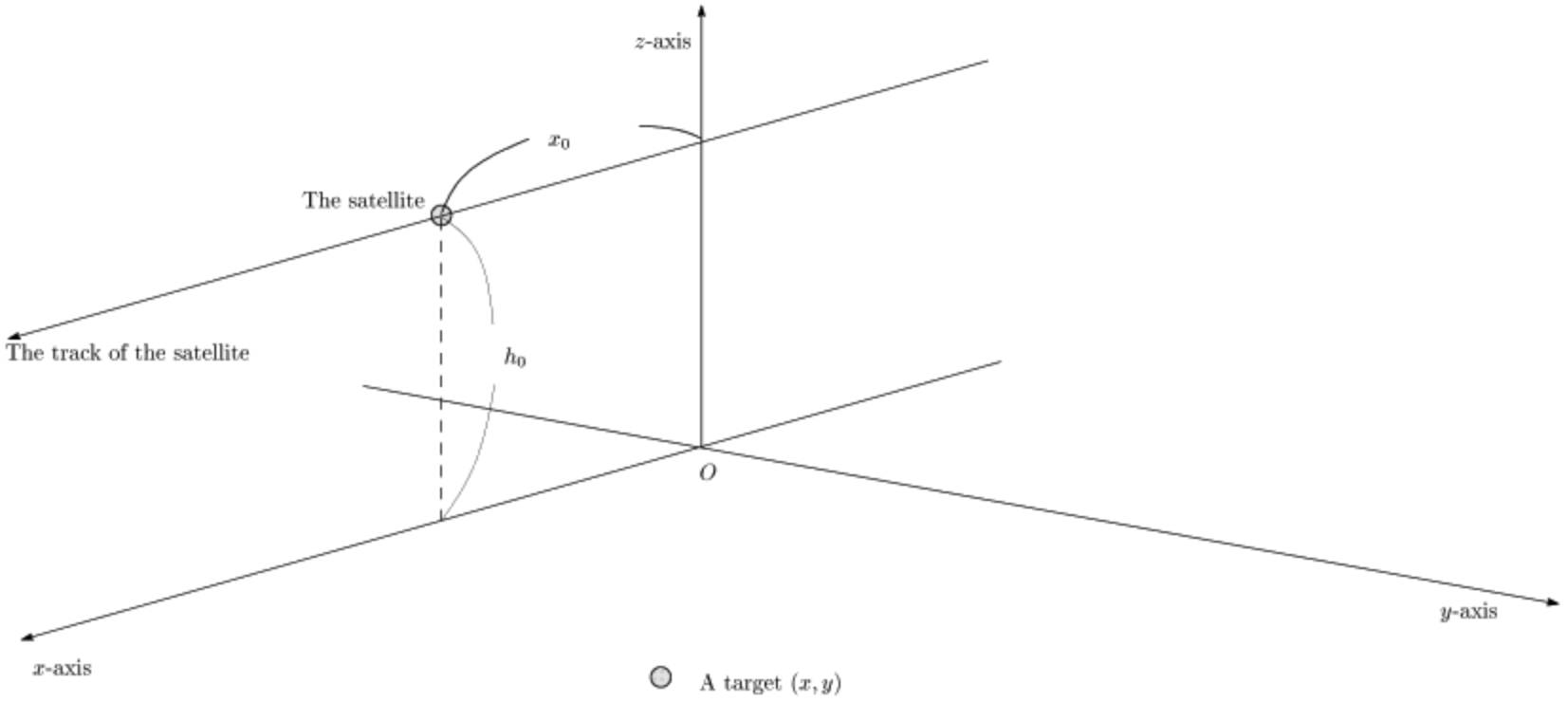

Figure 1: Relationship between the satellite and a point on the ground

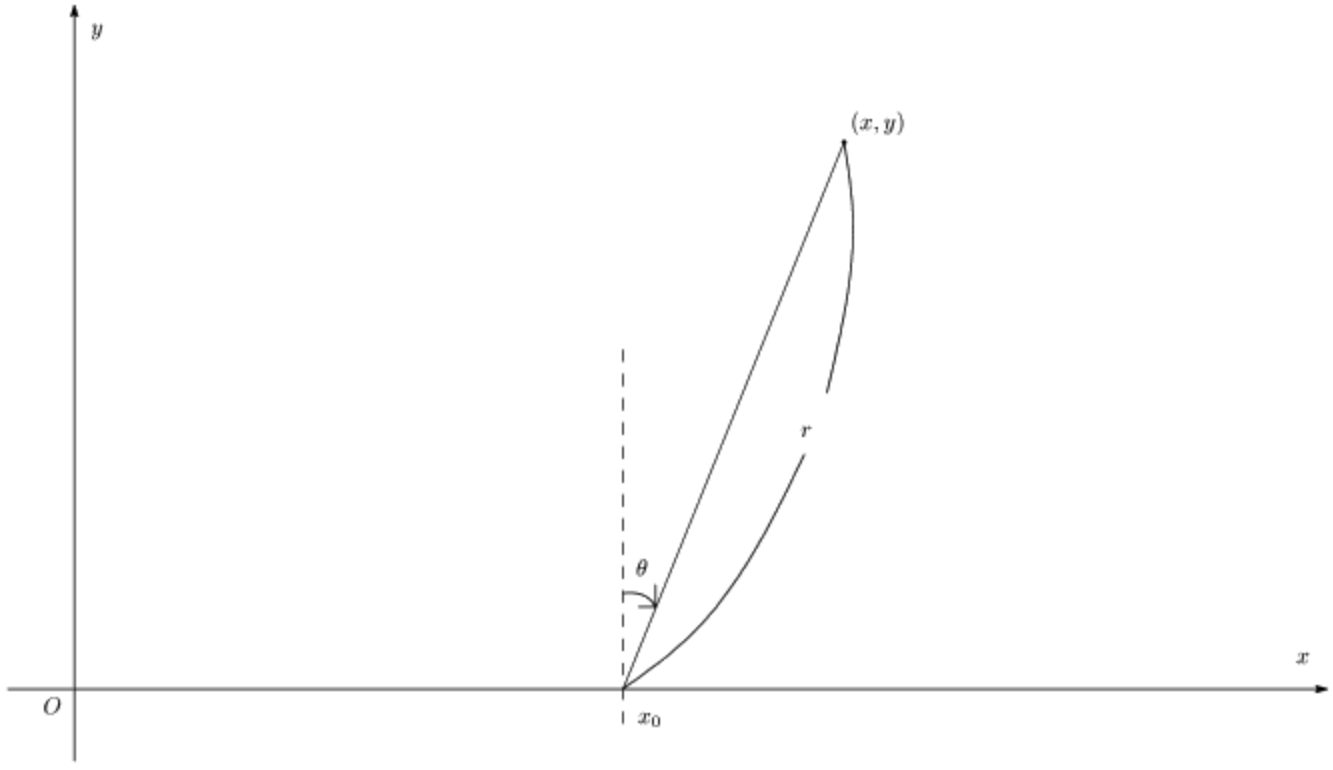

Figure 2 : local polar coordinate system

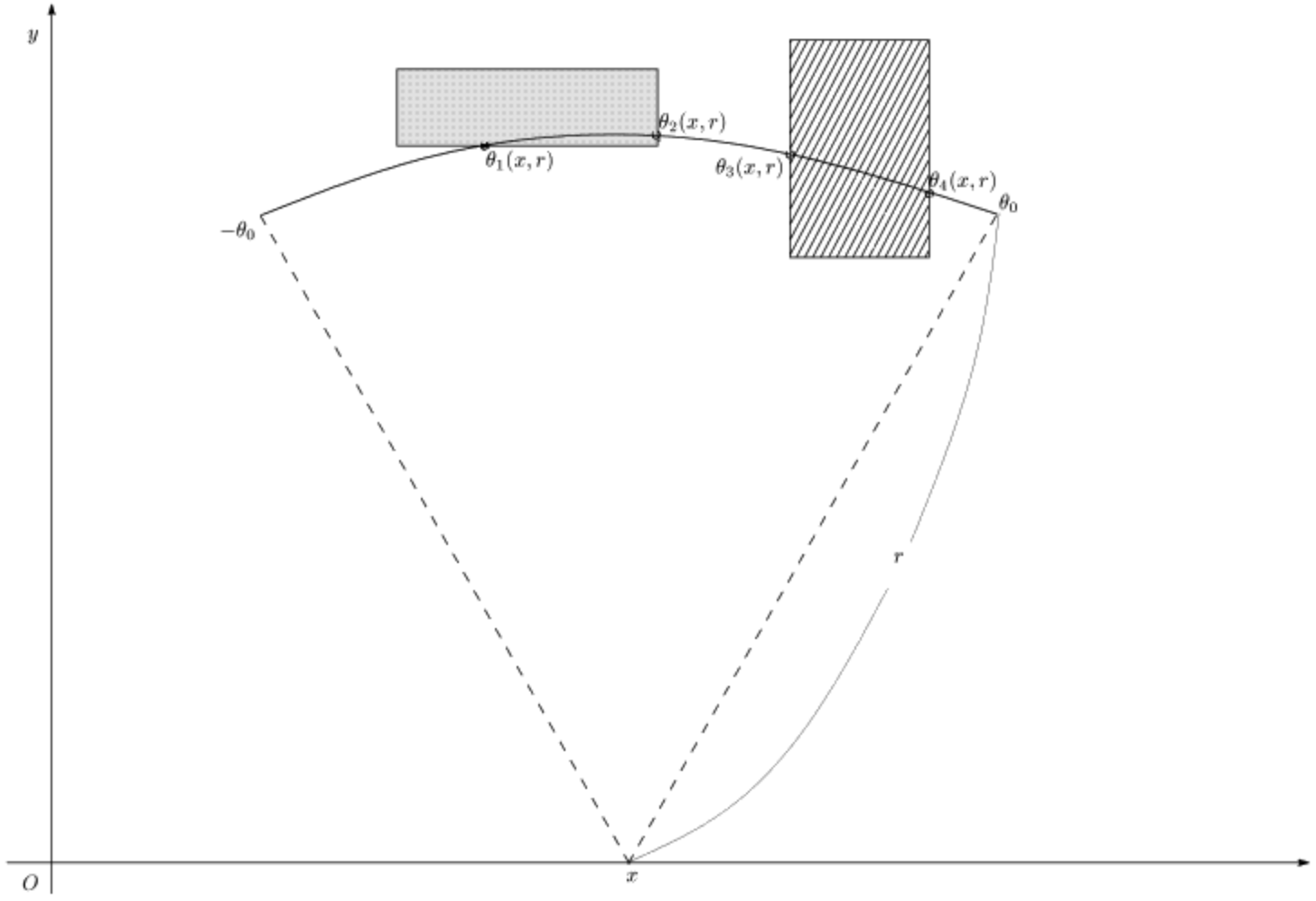

Figure 3 : Relation between $\theta_k(x,r)$ and objects on the ground surface.

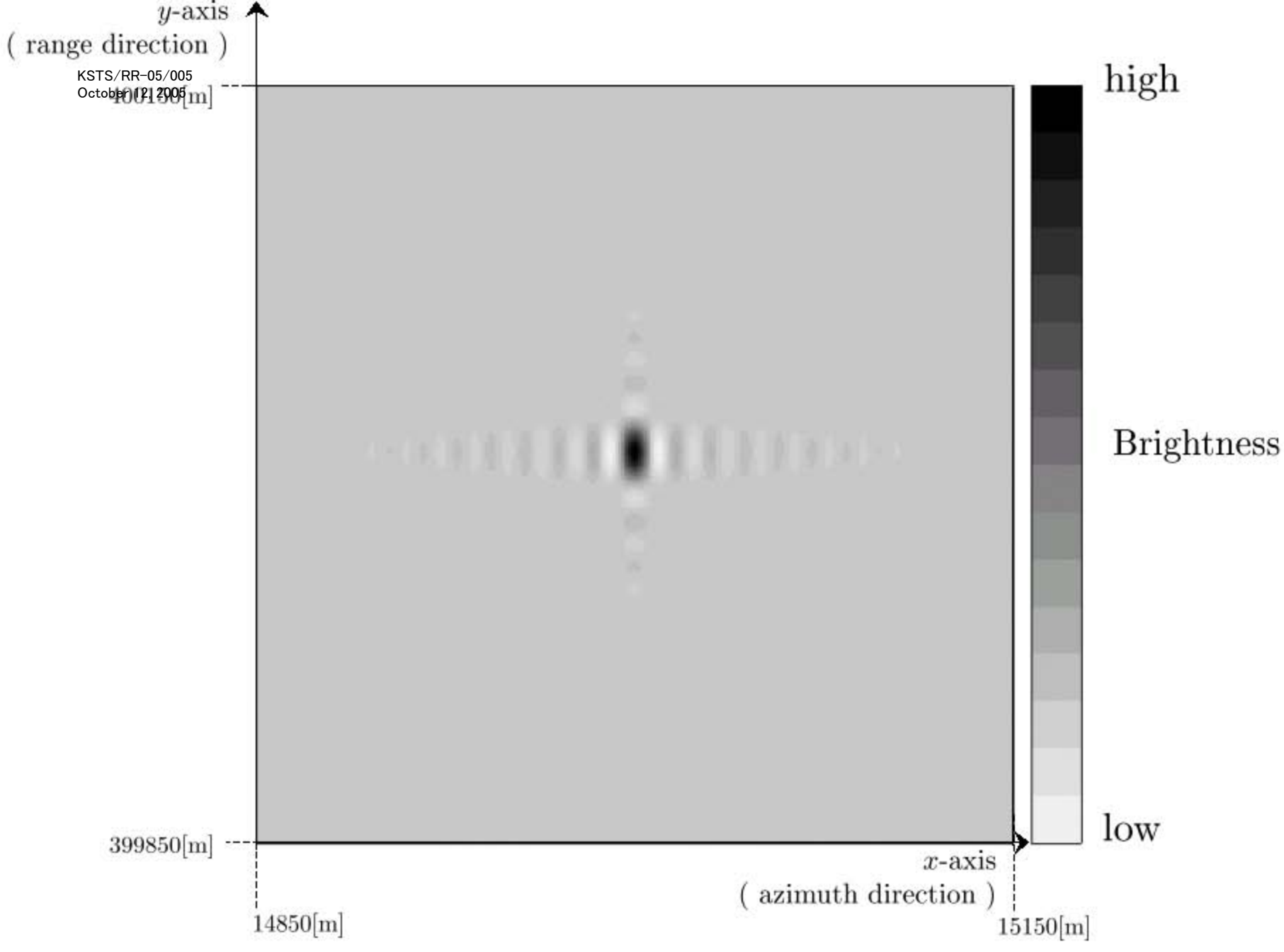

Figure 4: Ground reflection coefficient reconstructed by the pulse compression technique when there are two point targets on the ground.

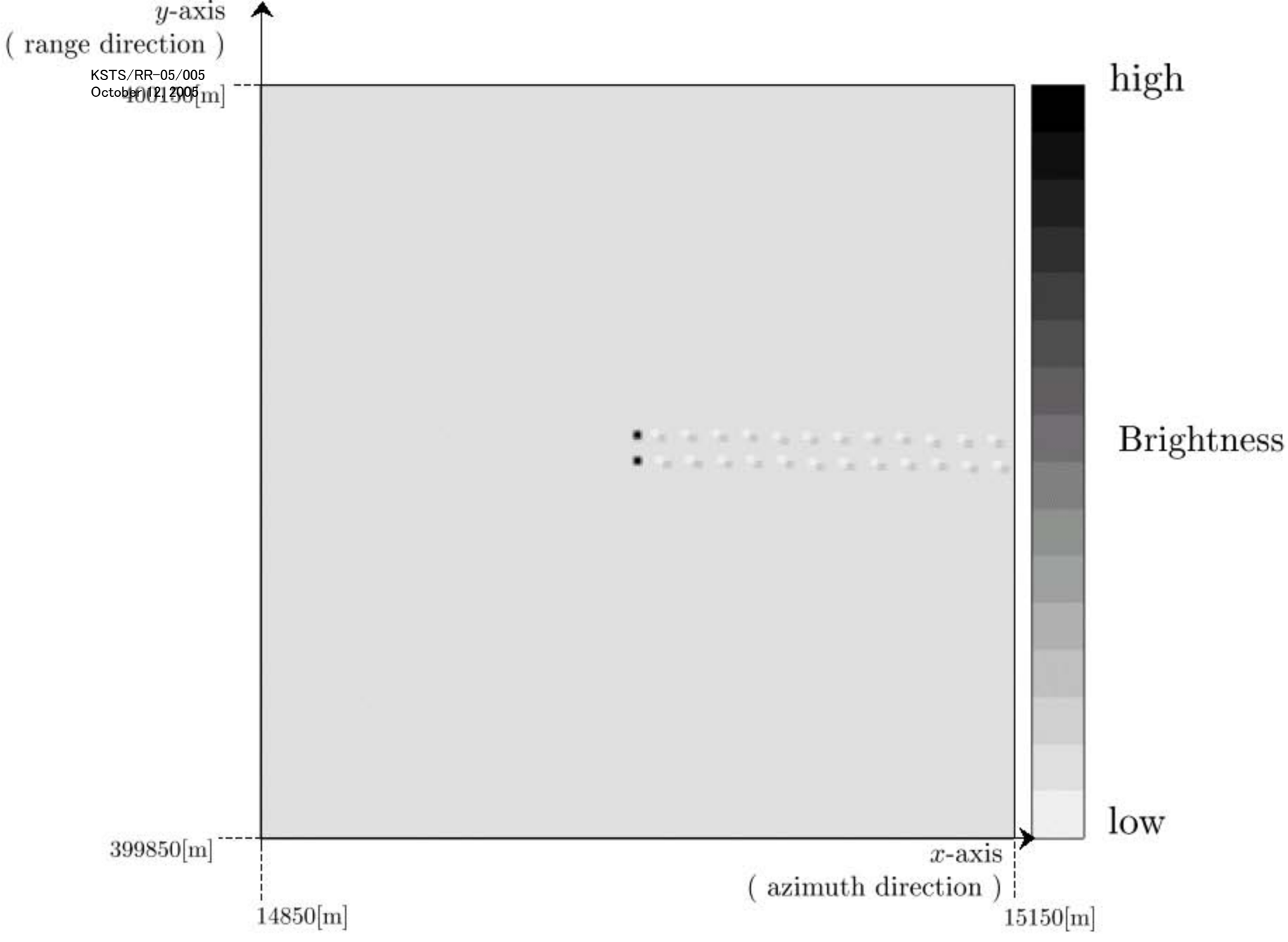

Figure 5: Ground reflection coefficient reconstructed by shape recovery method when there are two objects on the ground.

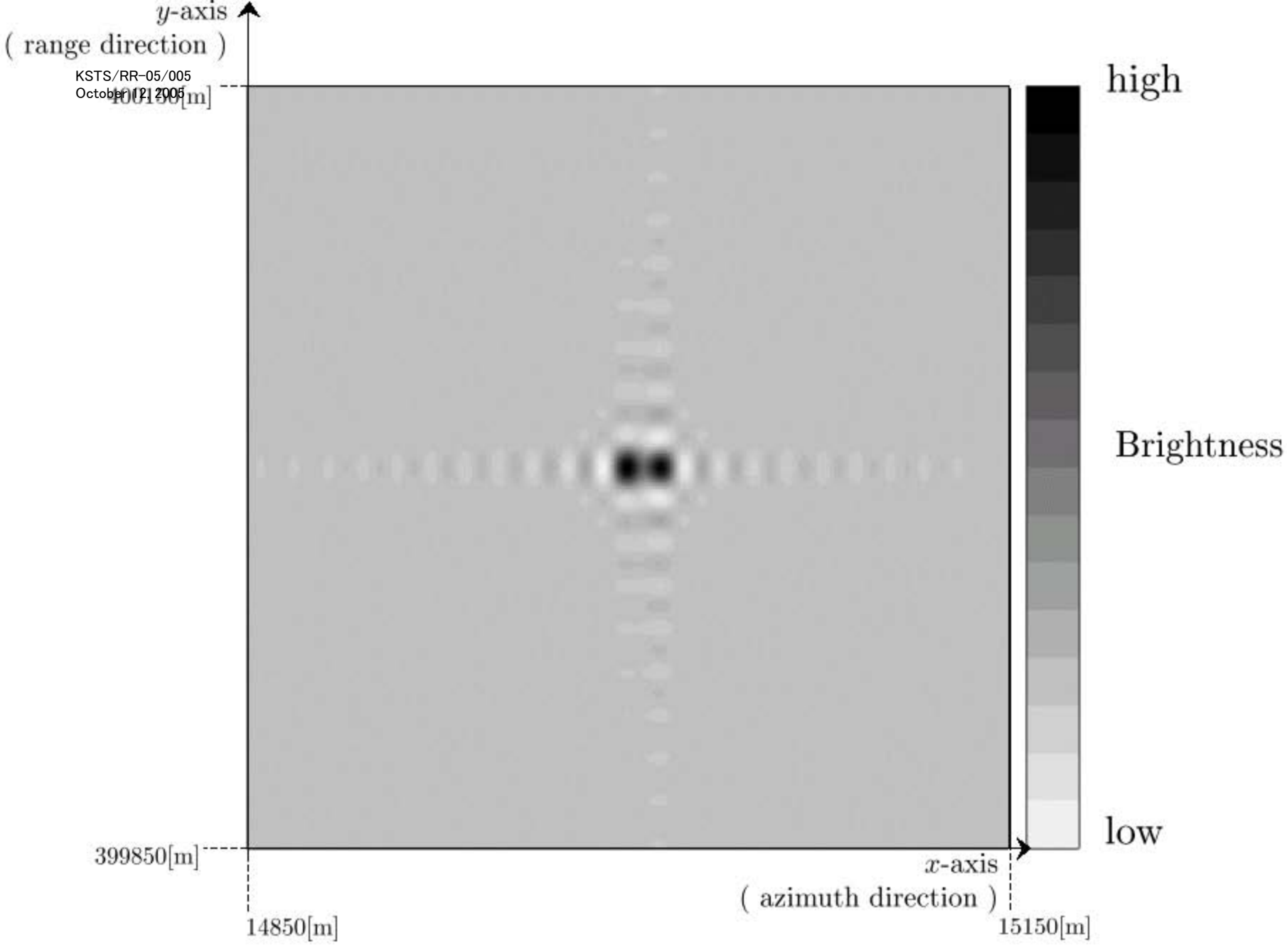

Figure 6: Ground reflection coefficient reconstructed by the pulse compression technique when there are two objects with different shapes on the ground.

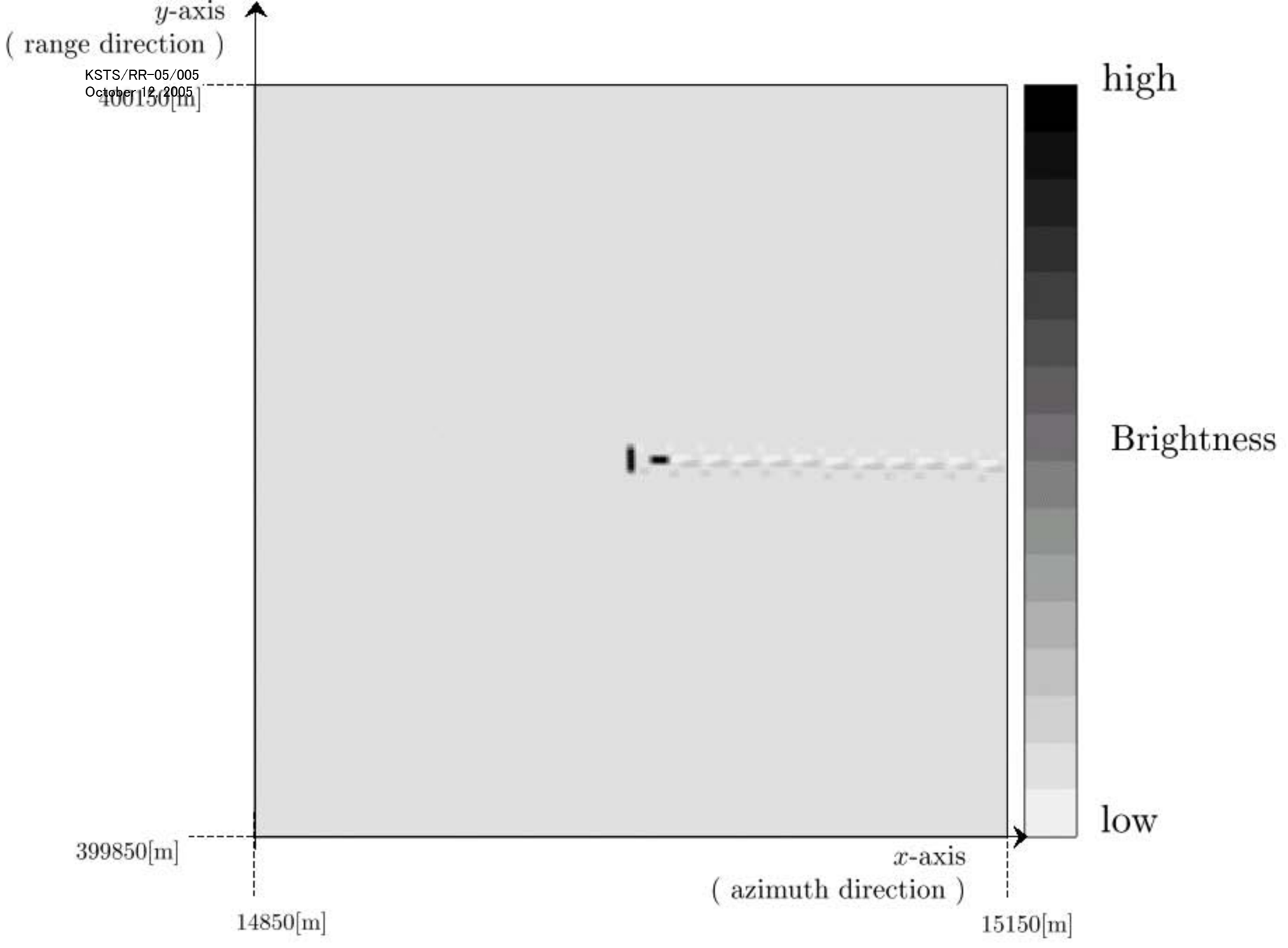

Figure 7: Ground reflection coefficient reconstructed by our method when there are two objects with different shapes on the ground.

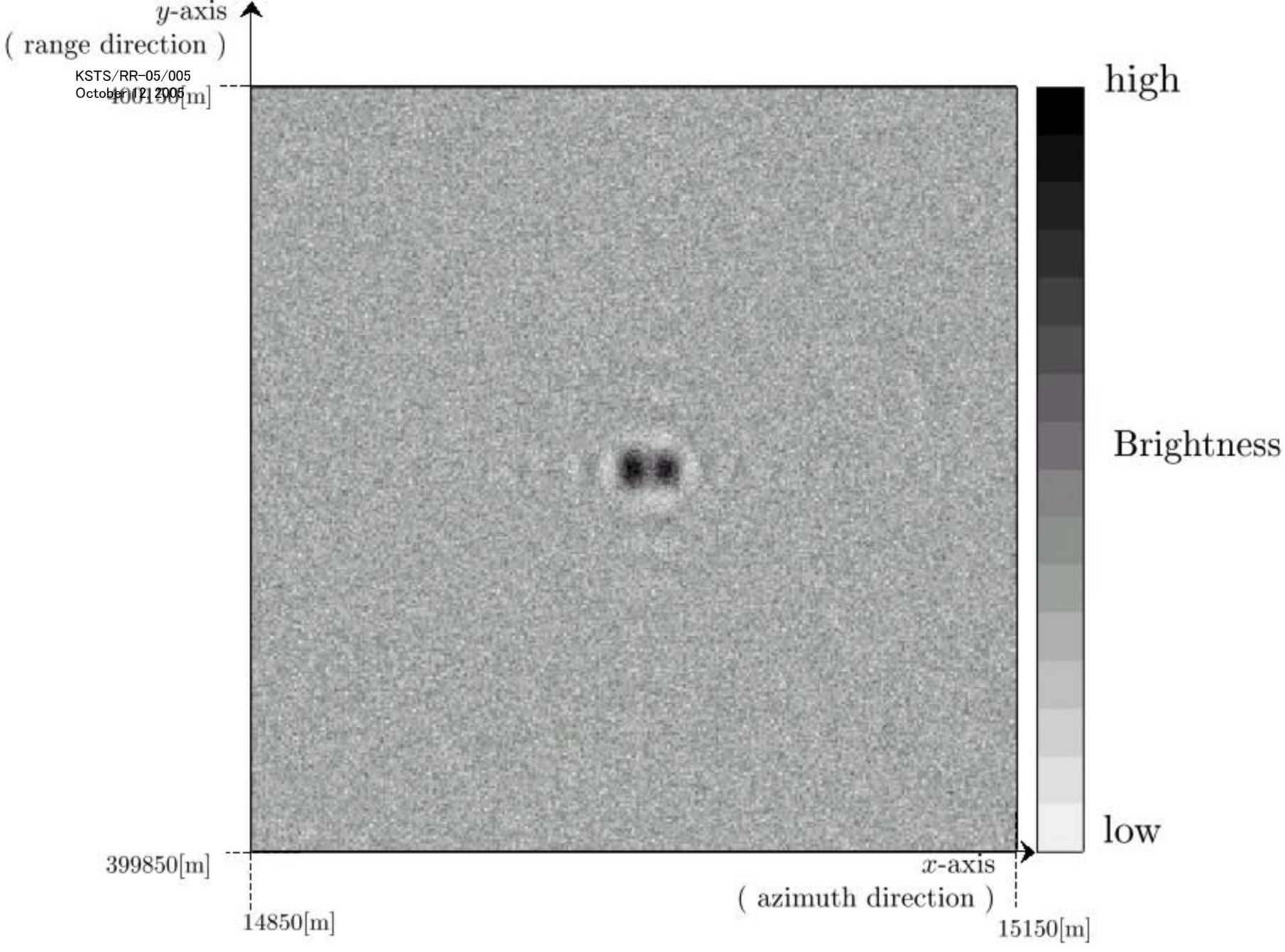

Figure 8: Ground reflection coefficient reconstructed by the pulse compression technique with noise when there are two objects with diferent shapes on the ground.

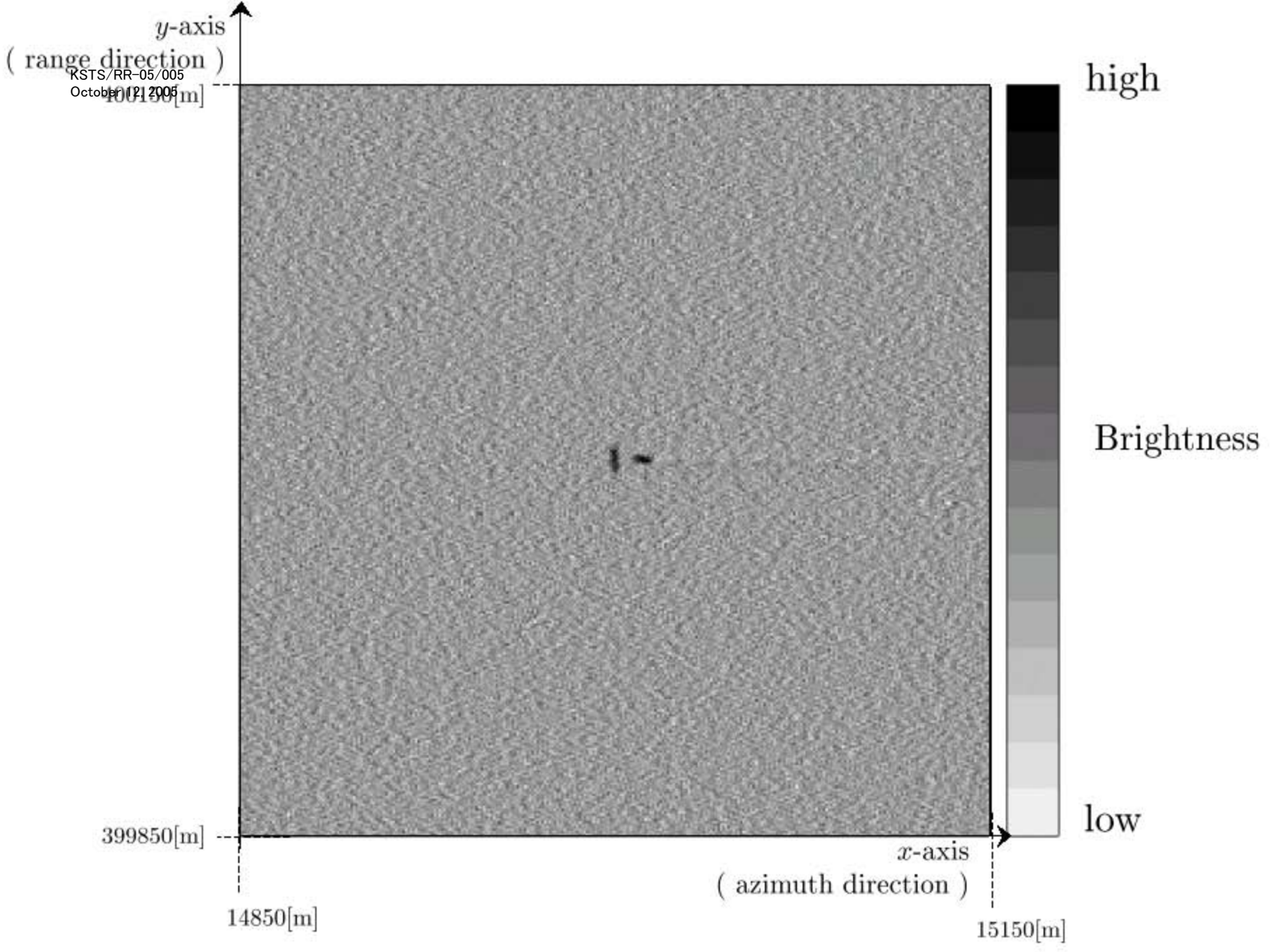

Figure 9: Ground reflection coefficient reconstructed by our method with noise when there are two objects with different shapes on the ground.

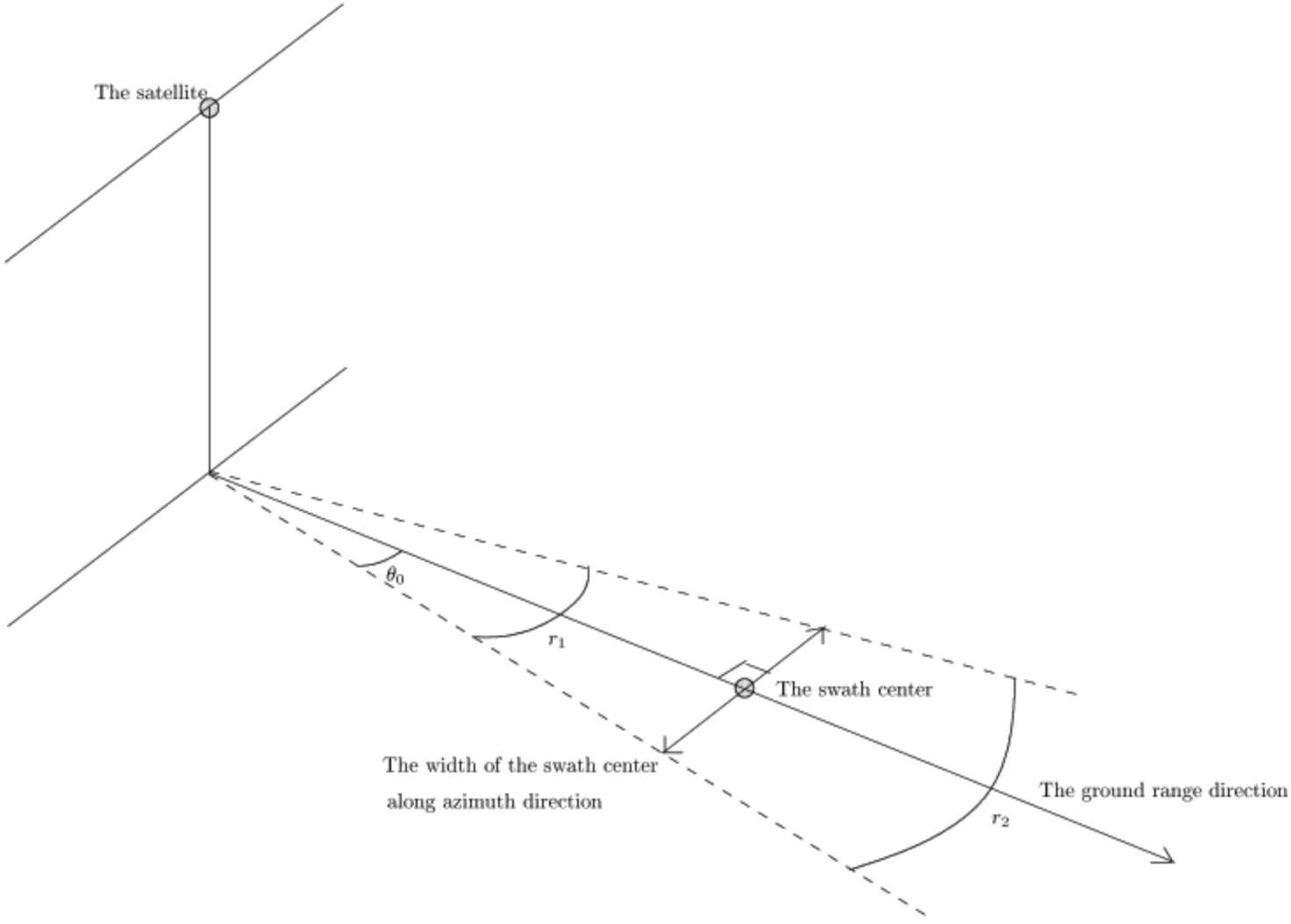

Figure 10 : Ground surface area irradiated by radar beam